

**eBook series: Frontiers in Nuclear and
Particle Physics
Special Issue: Multielectronic
Processes in Collisions Involving
Charged Particles and Photons with
Atoms and Molecules**

in press since 26 June 2017

August 11, 2018

Chapter 5

Multielectronic processes in particle and antiparticle collisions with rare gases

Claudia C. Montanari

Instituto de Astronomía y Física del Espacio, Consejo Nacional de Investigaciones Científicas y Técnicas, and Universidad de Buenos Aires, casilla de correo 67, sucursal 28, C1428EGA, Buenos Aires, Argentina.

Summary

In this chapter we analyze the multiple ionization by impact of $|Z| = 1$ projectiles: electrons, positrons, protons and antiprotons. Differences and similarities among the cross sections by these four projectiles allows us to have an insight on the physics involved. Mass and charge effects, energy thresholds, and relative importance of collisional and post-collisional processes are discussed. For this purpose, we performed a detailed theoretical-experimental comparison for single up to quintuple ionization of Ne, Ar, Kr and Xe by particles and antiparticles. We include an extensive compilation of the available data for the sixteen collisional systems, and the theoretical cross sections by means of the continuum distorted wave eikonal initial state approximation. We underline here that post-collisional ionization is decisive to describe multiple ionization by light projectiles, covering almost the whole energy range, from threshold to high energies. The normalization of positron and antiproton measurements to electron impact ones, the lack of data in certain cases, and the future prospects are presented and discussed.

Contents

Chapter 5	iii
0.1 Introduction	1
0.2 Theoretical description	2
0.2.1 The independent particle model for multiple ionization	3
0.2.2 CDW-EIS ionization probabilities by proton, antiproton, electron and positron impact	4
0.2.3 Auger type postcollisional ionization	5
0.3 Results and data	5
0.3.1 The multiple ionization of Ne	6
0.3.2 The multiple ionization of Ar	9
0.3.3 The multiple ionization of Kr	17
0.3.4 The multiple ionization of Xe	23
0.4 Concluding remarks and future prospects	32

List of Figures

1	Single ionization of Ne by $ Z = 1$ projectiles as a function of the impact energy, considering equal velocity for heavy and light particles. Curves: CDW-EIS results for proton (blue thin solid line), antiproton (red dotted line), electron (black thick solid line) and positron (orange dashed-line) impact. Symbols: details in the inset; the references are: for protons p+ [6, 8, 14, 15, 16, 20], for electrons e- [21, 22, 24, 25, 26], for positrons e+ [40, 45], and for antiprotons p- [16, 35].	7
2	Double ionization of Ne by $ Z = 1$ projectiles as a function of the impact energy, considering equal velocity for heavy and light particles. Curves: CDW-EIS results for proton (blue thin solid line), antiproton (red dotted line), electron (black thick solid line) and positron (orange dashed-line) impact. Symbols: details in the inset; the references are: for protons p+ [6, 8, 14, 15, 16, 19, 20], for electrons e- [21, 22, 24, 25, 26, 29, 30], for positrons e+ [45], and for antiprotons p- [35].	8
3	Triple ionization of Ne by $ Z = 1$ projectiles as a function of the impact energy, considering equal velocity for heavy and light particles. Curves: CDW-EIS results for proton (blue thin solid line), antiproton (red dotted line), electron (black thick solid line) and positron (orange dashed-line) impact. Symbols: details in the inset; the references are: for protons p+ [8, 14, 15, 16], for electrons e- [21, 22, 24, 25, 26, 29, 30], and for antiprotons p- [35].	10
4	Single ionization of Ar by $ Z = 1$ projectiles as a function of the impact energy, considering equal velocity for heavy and light particles. Curves: CDW-EIS results for proton (blue thin solid line), antiproton (red dotted line), electron (black thick solid line) and positron (orange dashed line) impact. Symbols: details in the inset; the references are: for protons p+ [9, 14, 15, 16, 19, 20], for electrons e- [21, 22, 24, 25, 26, 27, 28, 31], for positrons e+ [40, 42], and for antiprotons p- [16, 35, 36].	11

- 5 Double ionization of Ar by $|Z| = 1$ projectiles as a function of the impact energy, considering equal velocity for heavy and light particles. Curves: CDW-EIS results for proton (blue thin solid line), antiproton (red dotted line), electron (black thick solid line) and positron (orange dashed line) impact. Symbols: details in the inset; the references are: for protons p+ [6, 8, 9, 14, 15, 17, 18, 16, 19], for electrons e- [21, 22, 23, 24, 25, 26, 27, 28, 31], for positrons e+ [45], and for antiprotons p- [35]. 12
- 6 Triple ionization of Ar by $|Z| = 1$ projectiles as a function of the impact energy, considering equal velocity for heavy and light particles. Curves: CDW-EIS results for proton (blue thin solid line), antiproton (red dotted line), electron (black thick solid line) and positron (orange dashed-line) impact; black dashed-double-dotted line, direct triple ionization by electron impact. Symbols: details in the inset; the references are: for protons p+ [9, 14, 15, 16, 19, 20], for electrons e- [21, 22, 23, 24, 25, 26, 27, 28, 31, 32], and for antiprotons p- [35]. 13
- 7 Quadruple ionization of Ar by $|Z| = 1$ projectiles as a function of the impact energy, considering equal velocity for heavy and light particles. Curves: CDW-EIS results for proton (blue thin solid line), antiproton (red dotted line), electron (black thick solid line) and positron (orange dashed-line) impact. Symbols: details in the inset; the references are: for protons p+ [9, 15], and for electrons e- [21, 23, 25, 26, 27, 28, 31, 32]. 15
- 8 Quintuple ionization of Ar by $|Z| = 1$ projectiles as a function of the impact energy, considering equal velocity for heavy and light particles. Curves: CDW-EIS results for proton (blue thin solid line), antiproton (red dotted line), electron (black thick solid line) and positron (orange dashed-line) impact. Symbols: details in the inset; the references for electrons e- are [21, 23, 26, 27, 31, 32]. 16
- 9 Single ionization of Kr by $|Z| = 1$ projectiles as a function of the impact energy, considering equal velocity for heavy and light particles. Curves: CDW-EIS results for proton (blue thin solid line), antiproton (red dotted line), electron (black thick solid line) and positron (orange dashed-line) impact. Symbols: details in the inset; the references are: for protons p+ [6, 9, 14, 15, 20], for electrons e- [21, 22, 23, 24, 25, 26], for positrons e+ [45], and for antiprotons p- [35]. 17

- 10 Double ionization of Kr by $|Z| = 1$ projectiles as a function of the impact energy, considering equal velocity for heavy and light particles. Curves: CDW-EIS results for proton (blue thin solid line), antiproton (red dotted line), electron (black thick solid line) and positron (orange dashed-line) impact. Symbols: details in the inset; the references are: for protons p+ [6, 8, 9, 14, 15, 17, 18, 16, 19], for electrons e- [21, 22, 23, 24, 25, 26, 30], for positrons e+ [45], and for antiprotons p- [35]. 18
- 11 Triple ionization of Kr by $|Z| = 1$ projectiles as a function of the impact energy, considering equal velocity for heavy and light particles. Curves: CDW-EIS results for proton (blue thin solid line), antiproton (red dotted line), electron (black thick solid line) and positron (orange dashed-line) impact. Symbols: details in the inset; the references are: for protons p+ [9, 14, 15, 20], for electrons e- [21, 22, 23, 24, 25, 26, 30], and for antiprotons p- [35]. 20
- 12 Quadruple ionization of Kr by $|Z| = 1$ projectiles as a function of the impact energy, considering equal velocity for heavy and light particles. Curves: CDW-EIS results for proton (blue thin solid line), antiproton (red dotted line), electron (black thick solid line) and positron (orange dashed-line) impact. Symbols: details in the inset; the references are: for protons p+ [9, 15], and for electrons e- [21, 24, 25, 26, 30]. 21
- 13 Quintuple ionization of Kr by $|Z| = 1$ projectiles as a function of the impact energy, considering equal velocity for heavy and light particles. Curves: CDW-EIS results for proton (blue thin solid line), antiproton (red dotted line), electron (black thick solid line) and positron (orange dashed-line) impact. Symbols: details in the inset; the references are: for protons p+ [15], and for electrons e- [21, 23, 26, 30]. 22
- 14 Single ionization of Xe by $|Z| = 1$ projectiles as a function of the impact energy, considering equal velocity for heavy and light particles. Curves: CDW-EIS results for proton (blue thin solid line), antiproton (red dotted line), electron (black thick solid line) and positron (orange dashed-line) impact. Symbols: details in the inset; the references are: for protons p+ [9, 14, 18], for electrons e- [21, 22, 23, 24, 25, 26], for positrons e+ [42], and for antiprotons p- [35]. 24

- 15 Double ionization of Xe by $|Z| = 1$ projectiles as a function of the impact energy, considering equal velocity for heavy and light particles. Curves: CDW-EIS results for proton (blue thin solid line), antiproton (red dotted line), electron (black thick solid line) and positron (orange dashed-line) impact. Symbols: details in the inset; the references are: for protons p+ [9, 14, 18], for electrons e- [21, 22, 23, 24, 25, 26, 29, 30], for positrons e+ [45, 49, 48], and for antiprotons p- [35]. 26
- 16 Triple ionization of Xe by $|Z| = 1$ projectiles as a function of the impact energy, considering equal velocity for heavy and light particles. Curves: CDW-EIS results for proton (blue thin solid line), antiproton (red dotted line), electron (black thick solid line) and positron (orange dashed-line) impact. Symbols: details in the inset; the references are: for protons p+ [9, 14, 18], for electrons e- [21, 22, 23, 24, 25, 26, 29, 30], for positrons e+ [49, 50, 51], and for antiprotons p- [35]. 27
- 17 Quadruple ionization of Xe by $|Z| = 1$ projectiles as a function of the impact energy, considering equal velocity for heavy and light particles. Curves: CDW-EIS results for proton (blue thin solid line), antiproton (red dotted line), electron (black thick solid line) and positron (orange dashed-line) impact. Symbols: details in the inset; the references are: for protons p+ [9], for electrons e- [21, 23, 24, 25, 26, 29, 30], and for positrons e- [49]. 29
- 18 Quintuple ionization of Xe by $|Z| = 1$ projectiles as a function of the impact energy, considering equal velocity for heavy and light particles. Curves: CDW-EIS results for proton (blue thin solid line), antiproton (red dotted line), electron (black thick solid line) and positron (orange dashed-line) impact. Symbols: details in the inset; the references are: for protons p+ [9], and for electrons e- [21, 23, 24, 25, 26, 29, 30]. 30

0.1 Introduction

Multiple ionization is a challenging subject, which plays an important role in the knowledge of many-electron processes, such as multiple-electron transitions, collisional and post-collisional ionization or electron correlation effects. The goal of this contribution is to deepen in the study of the multielectronic processes by collision of $|Z| = 1$ particles and antiparticles. For this purpose we focused in the multiple ionization of the heaviest rare gases, Ne, Ar, Kr and Xe. We analyzed the differences and similarities in the cross sections of equal-charge versus equal-mass projectiles. The ionization cross sections by light (electrons and positrons) and heavy (protons and antiprotons) projectiles are quite different in the low and intermediate energy regions. On the contrary, in the high energy region all these cross sections converge. However, this convergence to proton impact values is different for antiprotons, positrons or electrons. A detailed knowledge of this tendency from intermediate to high impact energies is important because of the experimental normalization of relative cross sections of antiparticles to electron or to proton values. Classical reviews on particle and antiparticle collisions can be found in [1, 2, 3, 4, 5].

The theoretical description of the multiple ionization processes by these projectiles must consider the charge and mass effects, the projectile trajectories, and the energy thresholds. The post-collisional ionization (PCI) due to Auger-type processes following inner-shell ionization, enhance the final number of emitted electrons. For heavy projectiles this is important at high energies. For light projectiles, such as electrons and positrons, PCI dominates the highly-charged ion production in the whole energy range, even close to the energy threshold. The ionization by proton and electron impact has been studied since the early years of the development of atomic physics. However, the experimental data on multiple ionization by high energy protons could not be theoretically described until the last fifteen years [8, 9, 10, 11, 12]; and by electron impact only recently [13]. This was possible by a consistent inclusion of the branching ration for PCI within the independent electron model.

Multiple ionization is also a sensitive test for the experimental work. Measurements require highly advanced techniques to get all possible channels and final states. For protons, they must separate pure ionization from capture channels, which enhance the data in the intermediate energy region [6]. In the case of positron impact, the total ionization values at low energies include positronium formation [7]. On the other hand, the higher the order of ionization the smaller the cross sections. The quintuple ionization cross sections of Kr and Xe are of the order of the 10^{-19} cm² at high energies, while for Ar they are 10^{-20} cm² or even 10^{-21} cm².

The published experimental data of multiple ionization of Ne, Ar, Kr and

Xe by proton impact is profuse [6, 8, 9, 14, 15, 16, 17, 18, 19, 20]. Much more abundant are the measurements by electron impact. They include the pioneering works by Schram and co-workers in the 60s [21] to the present [22, 23, 24, 25, 26, 27, 28, 29, 30, 31, 32].

Instead, the experimental data by antiparticle is more scarce, what is reasonable. Antiprotons are produced in high-energy physics sources and then decelerated for atomic collisions experiments. This research has been developed by Knudsen and coworkers at CERN [16, 33, 34, 35, 36, 37], first in the low energy antiproton ring (LEAR) and nowadays in the antiproton decelerator (AD). A very recent *state of art* of antiproton impact ionization has been published by Kirchner and Knudsen [38]. In the case of positrons, most of the experimental publications report only values of single ionization [39, 40, 41, 42, 43], some articles include double or triple ionization measurements [44, 45, 46, 47, 48, 49, 50, 51], and only one paper quadruple ionization [49]. It is worth to mention that antiproton and positron values are normalized to electron impact ionization cross sections at high energies.

In this chapter we present a comparison of the multiple ionization cross sections by impact of electrons, positrons, protons and antiprotons. We consider the rare gases Ne, Ar, Kr and Xe, and final charge states from +1 to +3 (Ne), and +5 (Ar, Kr and Xe). The comparison includes the theoretical results obtained by employing the continuum distorted wave eikonal initial state approximation in [12, 13, 52, 53], and the available experimental measurements. The extensive compilation of data for the four projectiles and the four targets included here, allow us to have a wide vision of the experimental *state of art*, and some future prospects.

0.2 Theoretical description

The theoretical description of the multiple ionization reviewed in this chapter relies on three approximations:

1. The **independent particle model** (IPM): the ejected electrons ignore each other, neglecting the correlation in the final state and the changes in the target potential due to the successive loss of electrons. Under this assumption, the probability of multiple ionization can be expressed as a multinomial combination of independent ionization probabilities.
2. The **continuum distorted wave eikonal initial state** (CDW-EIS) approximation [54, 55]. This is a proved model to describe intermediate and high energy multiple ionization by protons and antiprotons [12, 52]. In [13, 53], the CDW-EIS is adapted to describe ionization by electrons

or positrons, by taking into account the finite momentum transferred, the non-linear trajectory and the mass effect. Light particle ionization is characterized by the sharp energy thresholds, which are different for single to quintuple ionization. The results in [53] include the different thresholds of energy within the multinomial expansion following [56].

3. The **post-collisional ionization (PCI), independent of the projectile**. Thus, it is included within the multinomial expression in a semi empirical way following [8, 10], using the experimental branching ratios of the charge-state distribution after a single initial vacancy. Present formalism is explained in [12]. A detailed compilation of these branching ratios is available in [13].

In what follows the implications of these approximations on the calculations are summarized. More details of them can be found in the mentioned references.

0.2.1 The independent particle model for multiple ionization

Within the IPM, the probability of direct ionization of exactly q_j electrons of the j subshell as a function of the impact parameter b , $P_{(q_j)}(b)$, is obtained as a multinomial distribution of the ionization probabilities $p_j(b)$ given by

$$P_{(q_j)}(b) = \binom{N_j}{q_j} [p_j(b)]^{q_j} [1 - p_j(b)]^{N_j - q_j}, \quad (1)$$

where N_j is the total number of electrons in the subshell. If n electrons are ionized from the different shells, $n = \sum_j q_j$, then the total probability of direct ionization is

$$P_{(n)}(b) = \sum_{q_1 + q_2 + \dots = n} \prod_j P_{(q_j)}(b). \quad (2)$$

and the cross section corresponding to the direct ionization of exactly n electrons is

$$\sigma_n = \int P_{(n)}(b) 2\pi b db. \quad (3)$$

The main and more sensitive values of these calculations are the ionization probabilities as function of the impact parameter, $p_j(b)$. Different models have been employed in the last fifteen years to obtain these $p_j(b)$ for multiple ionization calculations, by the groups of Montenegro [8, 9, 12, 57, 58, 59, 60], Kirchner [10, 61, 62, 63, 64, 65], Rivarola [11, 66, 67], and Miraglia [12, 13, 52, 53, 68, 69].

0.2.2 CDW-EIS ionization probabilities by proton, antiproton, electron and positron impact

We review here the results for proton, antiproton, electron and positron impact multiple ionization in [12, 13, 52, 53]. These results employ the CDW-EIS code by Miraglia [54]. Details of these calculations are in [52, 54]. The aim is to discuss the scope and limitations of this model to deal with particle-antiparticle and heavy-light projectile effects.

The CDW-EIS ionization probabilities $p_j(b)$ as function of the impact parameters are the seeds to be introduced in the multinomial expression given by (1). As expected, these results tend to the first Born approximation ones at sufficiently high impact energies [52]. In fact, the extension of the theoretical results for impact velocities $v > 8$ a.u. in [12, 13, 52, 53] is achieved using the first Born approximation.

On the other hand, the CDW-EIS results for light projectiles in [13, 53] were obtained by adapting the CDW-EIS model for equal-charged light projectiles, i.e. protons \rightarrow positrons; antiprotons \rightarrow electrons. This calculation accounted for the finite momentum transferred, the non-linear trajectory (very different for positrons and electrons due to the repulsive or attractive potentials), and the minimum energy for ionization. A detailed explanation and the corresponding equations can be found in [13].

The CDW-EIS results in [12, 13, 52, 53] describe *pure* ionization of the target. No electron transfer or transfer followed by projectile electron loss is included. These processes are possible only for positive projectiles, and may enlarge the experimental cross sections at low energies.

Ionization processes present a sharp energy threshold: ionization is not possible for projectile energies below the binding energy of the target outer electrons. The threshold for each shell of electrons must be taken into account within the multinomial expression (1). One of the differences between light and heavy projectiles is that, on equal impact velocity, light projectiles have impact energies of the order of the target binding energies or even lower. This is the main cause of differences between ionization cross sections by light and heavy projectiles at intermediate to low energies.

Experimentally the threshold or appearance energy is well known and measured in electron and positron-impact ionization. For n -fold ionization the experiments indicate that this appearance energy is much greater than n times the binding energy of the outermost electrons. This was analyzed in [56] considering not only the energy gap, but also the mean velocity of the outgoing electrons in a semi-classical way. This proposal was included in the multiple ionization calculations by electron and positron impact in [53]. Although the threshold itself is rather well described, the theoretical model cannot be em-

ployed close to the energy threshold. The CDW-EIS approximation fails at low impact energies, i.e. when the energy loss by the projectile is comparable to the impact energy. We will return to this later in this chapter.

0.2.3 Auger type postcollisional ionization

The PCI is the rearrangement of the target atom after inner-shell ionization. Different processes (shake off, Auger decay and emission) are involved in the emission of one or more electrons long after the collision. Following Cavalcanti *et al* [8] and Spranger and Kirchner [10], the PCI is included inside the binomial equation (1) in a semi-empirical way by using experimental branching ratios of charge state distribution after single photoionization. The deeper the initial hole, the greater the number of electrons in PCI.

The branching ratios $F_{j,k}$ are the probabilities of losing k electrons in PCI after single ionization of the j subshell. They correspond to time delayed processes that only depend on the target. A detailed compilation of the experimental branching ratios $F_{j,k}$ for Ne, Ar, Kr and Xe available in the literature is tabulated in [13]. It is interesting to note that they verify the unitary condition, $\sum_{k=0}^{k_{max}} F_{j,k} = 1$. In [12] the branching ratios are introduced in (1) as follows

$$P_{(q_j)}(b) = \binom{N_j}{q_j} [p_j(b) \sum_{k=0}^{k_{max}} F_{j,k}]^{q_j} [1 - p_j(b)]^{N_j - q_j}. \quad (4)$$

Afterwards, the addition of probabilities is arranged in order to put together those terms that contribute to the same final number of emitted electrons. New probabilities of exactly n emitted electrons are obtained, including direct ionization and PCI, $P_{(n)}^{PCI}$ (see section 2.3 in [12] for details). Thus, the corresponding cross sections of n -fold ionization including PCI are

$$\sigma_n^{PCI} = \int P_{(n)}^{PCI}(b) 2\pi b db. \quad (5)$$

0.3 Results and data of particle and antiparticle ionization: charge and mass effects

What follows is a revision of the theoretical CDW-EIS results for multiple ionization of Ne, Ar, Kr and Xe by protons and antiprotons [52], electrons [13], and positrons [53]. This is achieved by comparing and analyzing the cross sections for the four $|Z| = 1$ projectiles together, and contrasting them with the experimental data available in the literature. The comparison is performed on

equal impact velocities, and is plotted as a function of the corresponding electron impact energy. The change to proton impact energies is straightforward, just an m_p/m_e factor (the ratio of masses of heavy and light projectiles).

In the following sections the results for Ne, Ar, Kr and Xe are presented. We will note that the threshold for light particles is quite well described by the theory. However, we will focus on the description of the intermediate to high impact energy processes that is the range of validity of the CDW-EIS.

0.3.1 The multiple ionization of Ne

In figures 1-3 we plotted together the CDW-EIS results for proton, antiproton, electron, and positron impact ionization [52, 13, 53], for final Ne^+ to Ne^{+3} . We do not pretend to extend the validity of the IPM for Ne (ten bound electrons) beyond the triple ionization [60]. Changes in the target potential may be significant in this case. On the contrary, for targets with larger number of bound electrons, the IPM is expected to work.

Ne single ionization

In figure 1 we include the theoretical curves and the experimental measurements for the single ionization cross sections of Ne by protons (p+), antiprotons (p-), electrons (e-), and positrons (e+). It can be observed that the main difference between heavy and light projectiles are the lower values at intermediate and low energies, and the sharp threshold around 23 eV. Instead, all the results converge at high energies. The intermediate energy region is the most interesting one. We note that for equal mass, the values for projectiles with charge $Z = -1$ are below the $Z = +1$ ones. It could be said that the ionization of Ne is more effective by positive charges.

The theoretical description is rather good for the heavy projectiles. In the case of protons, below the maximum the agreement is fine only with the data by DuBois [6] who separates pure ionization and capture. This may be the difference between DuBois [6] data and the recent Sarkadi *et al* [20] experimental values at intermediate to low energies. In the case of antiprotons we remark the good agreement with Andersen measurements at high energies [16]. Instead, the data by Paludan [35] are somewhat below the predictions, but the tendency is correct. For single-ionization by light particles, the theoretical values overestimate around the maximum, and describe nicely the measurements at high energies.

The normalization of antiparticle cross sections is a point of discussion [53]. The experimental cross sections by positrons and antiprotons are mostly relative values normalized to well known and tested high energy electron impact

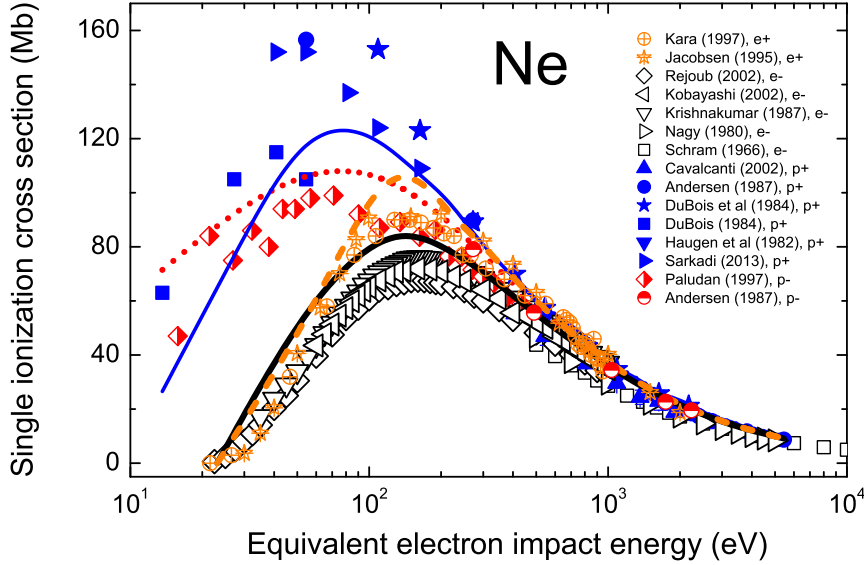


Figure 1: Single ionization of Ne by $|Z| = 1$ projectiles as a function of the impact energy, considering equal velocity for heavy and light particles. Curves: CDW-EIS results for proton (blue thin solid line), antiproton (red dotted line), electron (black thick solid line) and positron (orange dashed-line) impact. Symbols: details in the inset; the references are: for protons p+ [6, 8, 14, 15, 16, 20], for electrons e- [21, 22, 24, 25, 26], for positrons e+ [40, 45], and for antiprotons p- [16, 35].

data, such as Rapp *et al* [70], Sorokin *et al* [71], or Krishnakumar *et al* [24]. For example, the positron data by Kara *et al* [45] and antiproton data by Paludan *et al* [35] are both normalized to electron impact data by Krishnakumar *et al* [24] at 800-1000 eV. The comparison displayed in figure 1 shows that for the theoretical model, antiprotons and positrons tend faster to proton values than to electron ones at high energies. At 400 eV proton, antiproton and positron curves are together and 10% above electron impact values. Even around 1000 eV the electron single ionization is still a little below the rest. This implies that antiproton and positron relative values could be normalized to total proton-impact ionization cross sections, such as those by Rudd *et al* [72], at no so high energies.

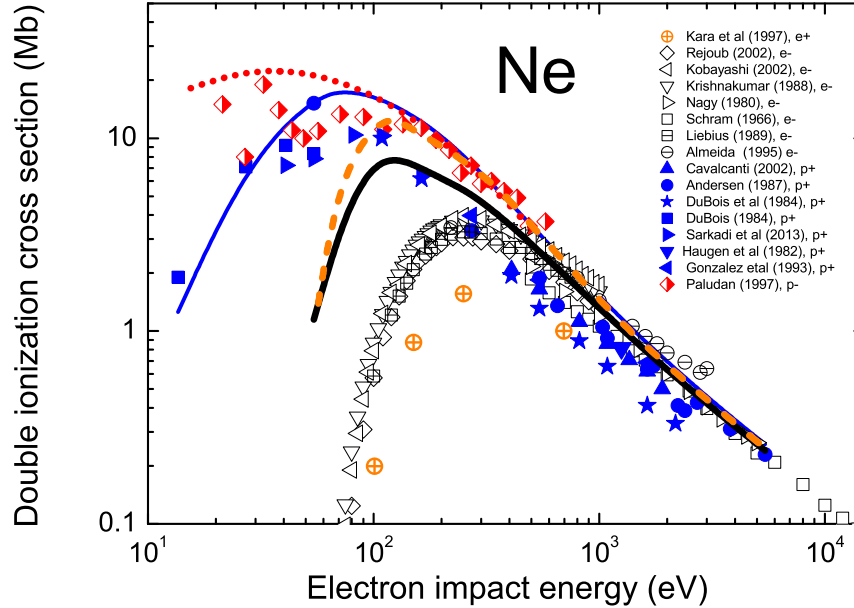


Figure 2: Double ionization of Ne by $|Z| = 1$ projectiles as a function of the impact energy, considering equal velocity for heavy and light particles. Curves: CDW-EIS results for proton (blue thin solid line), antiproton (red dotted line), electron (black thick solid line) and positron (orange dashed-line) impact. Symbols: details in the inset; the references are: for protons p+ [6, 8, 14, 15, 16, 19, 20], for electrons e- [21, 22, 24, 25, 26, 29, 30], for positrons e+ [45], and for antiprotons p- [35].

Ne double ionization

In figure 2 we display the double ionization of Ne. We use the logarithmic scale to emphasize the fall down and convergence at high energies, which is much more drastic than for single-ionization.

The double ionization cross sections by antiprotons at intermediate to low velocities, i.e. $v < 2.3$ a.u. are higher than by proton impact. Inverse to single ionization. And this reversal can be seen in the data and in the theoretical description too. Another point to remark in figure 2 is that theoretically, above 200 eV (electron impact) the proton, antiproton and even positron curves converge to a single value. Instead, for electron impact the convergence is above 600 eV. Experimentally, the positron data are below the electron measurements. It is not clear how much it influences the normalization of the single ionization measurements of positrons to electron-impact data at the level of

the double ionization.

At high energies, the description is actually good. Our values include the post-collisional Auger and shake off processes. At 3 keV the PCI contribution is 60% of the total double ionization (see figure 2 in [53]). At intermediate energies, the theoretical curves clearly overestimate the electron and positron-impact data. This is related to the inclusion of PCI due to shake-off of the outer shell electrons of Ne, as explained in [13]. This is an interesting open topic: The inclusion of PCI allows us to describe the high energy region, but it produced too high values at intermediate energies. On the contrary, if only direct double ionization is considered, the maximum for electron impact cross section and the energy threshold are better described, but the high energy measurements are undervalued.

Ne triple ionization

The triple ionization cross sections of Ne are displayed in figure 3. The theoretical results for proton and antiproton triple ionization are rather good. They clearly show that antiprotons produce larger triple ionization for energies around the maximum than protons. Note that this is exactly the opposite for single ionization.

The comparison of the cross sections by heavy and light projectiles shows the expected lower values for light projectiles and the convergence at high energies. The CDW-EIS results for light projectiles overestimate the measurements near the energy threshold. This is partially due to the overestimation of the shake-off contribution, and partially due to being in the limit of validity of the model, as mentioned previously in this chapter.

It is very interesting to mention that the high energy data could not be described if the postcollisional contribution to triple ionization (initial ionization of inner shells and rearrangements processes) is not included [13]. This contribution is important above 400 eV, being 90% of the triple ionization cross sections at 1 keV.

0.3.2 The multiple ionization of Ar

We analyze in this section the Ar multiple ionization, from single to quintuple. In figures 4-8 we displayed together the CDW-EIS results for proton, antiproton, electron and positron in Ar [52, 13, 53], and an updated compilation of experimental data for the four projectiles.

In the following figures it will be noted that the theoretical description shows better agreement with the measurements than for Ne. This behavior is enhanced for heavier targets, as we will observe for Kr and Xe in the following

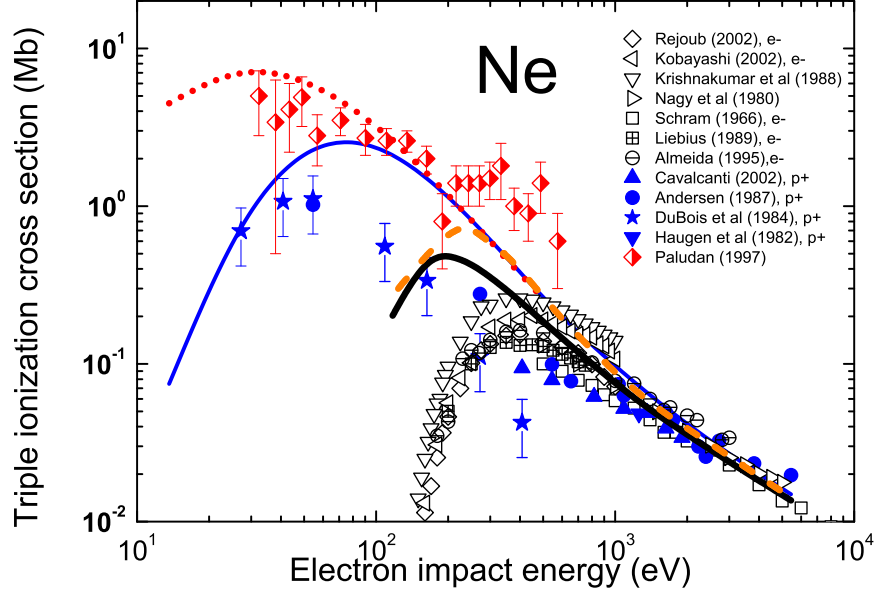


Figure 3: Triple ionization of Ne by $|Z| = 1$ projectiles as a function of the impact energy, considering equal velocity for heavy and light particles. Curves: CDW-EIS results for proton (blue thin solid line), antiproton (red dotted line), electron (black thick solid line) and positron (orange dashed-line) impact. Symbols: details in the inset; the references are: for protons p+ [8, 14, 15, 16], for electrons e- [21, 22, 24, 25, 26, 29, 30], and for antiprotons p- [35].

sections. The IPM works better to describe the multiple ionization in multi-electronic targets, so that the number of loose electrons is much smaller than the number of bound electrons.

Ar single ionization

In figure 4 the single ionization of Ar by the four $|Z| = 1$ projectiles is displayed. The good description of the experimental values by the CDW-EIS can be noted. The proton impact measurements by Andersen *et al*[16] and by Sarkadi *et al* [20] at impact velocities below 2.5 a.u. are clearly higher than the theoretical values. It may be possible that these single ionization measurements by proton impact include capture, enhancing the number of measured Ar^+ . Obviously, the antiproton measurements are pure ionization, and capture is not possible.

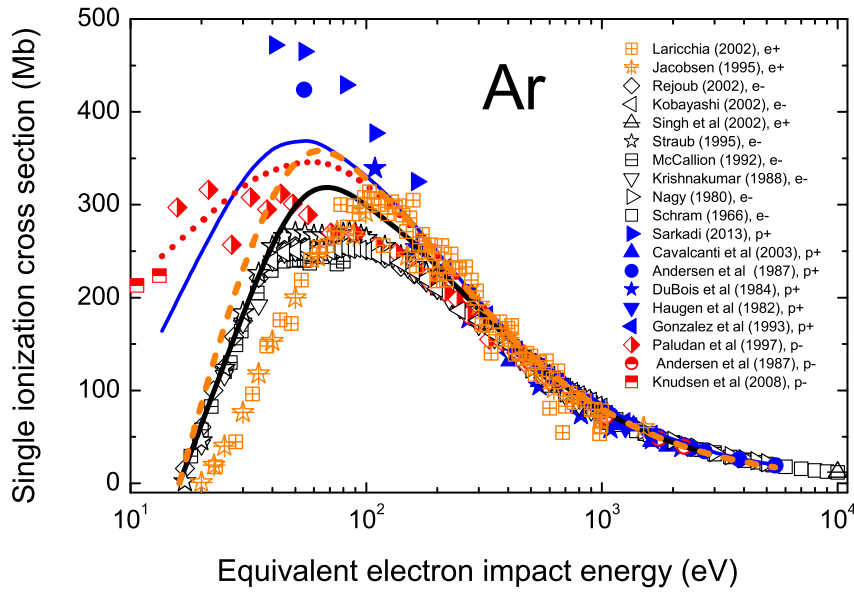


Figure 4: Single ionization of Ar by $|Z| = 1$ projectiles as a function of the impact energy, considering equal velocity for heavy and light particles. Curves: CDW-EIS results for proton (blue thin solid line), antiproton (red dotted line), electron (black thick solid line) and positron (orange dashed line) impact. Symbols: details in the inset; the references are: for protons p+ [9, 14, 15, 16, 19, 20], for electrons e- [21, 22, 24, 25, 26, 27, 28, 31], for positrons e+ [40, 42], and for antiprotons p- [16, 35, 36].

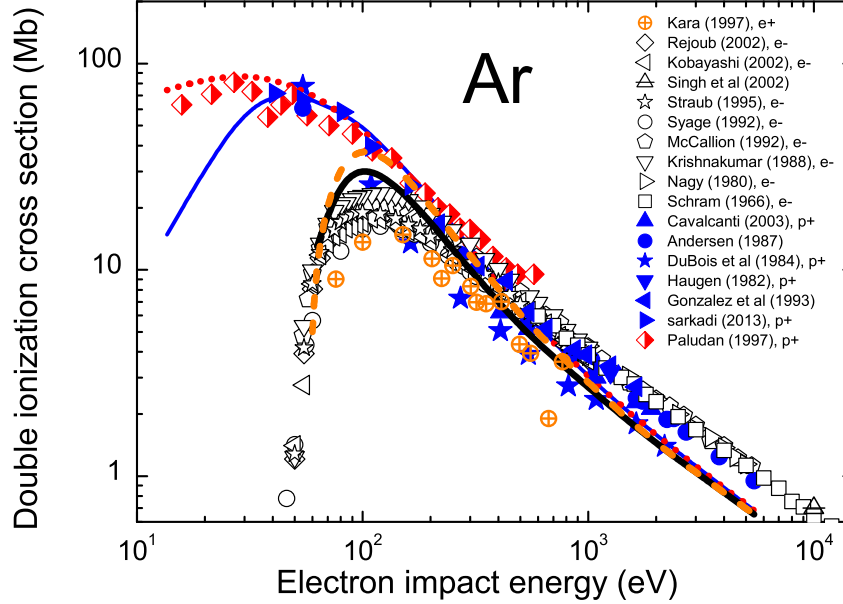


Figure 5: Double ionization of Ar by $|Z| = 1$ projectiles as a function of the impact energy, considering equal velocity for heavy and light particles. Curves: CDW-EIS results for proton (blue thin solid line), antiproton (red dotted line), electron (black thick solid line) and positron (orange dashed line) impact. Symbols: details in the inset; the references are: for protons p+ [6, 8, 9, 14, 15, 17, 18, 16, 19], for electrons e- [21, 22, 23, 24, 25, 26, 27, 28, 31], for positrons e+ [45], and for antiprotons p- [35].

In the high energy region, the convergence of the proton, antiproton, positron and electron measurements and also of the theoretical curves, is clearly above 300 eV. Again, our model predicts that the ionization by positrons tends to antiproton and proton values at lower energies than to the electron impact values. In the case of Ar, this tendency is also found in the experimental data by Laricchia and coworkers [42, 40].

Ar double ionization

In figure 5 the double ionization of Ar is shown. The general description obtained with the CDW-EIS for the heavy and the light projectiles is good. Though this model is not capable of describing the low energy processes, the

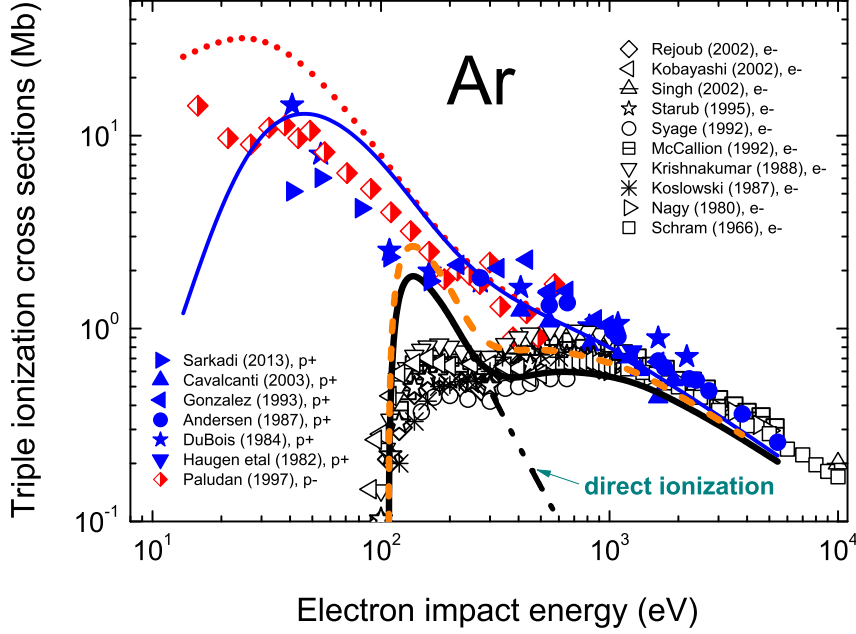


Figure 6: Triple ionization of Ar by $|Z| = 1$ projectiles as a function of the impact energy, considering equal velocity for heavy and light particles. Curves: CDW-EIS results for proton (blue thin solid line), antiproton (red dotted line), electron (black thick solid line) and positron (orange dashed-line) impact; black dashed-double-dotted line, direct triple ionization by electron impact. Symbols: details in the inset; the references are: for protons p+ [9, 14, 15, 16, 19, 20], for electrons e- [21, 22, 23, 24, 25, 26, 27, 28, 31, 32], and for antiprotons p- [35].

results are quite good in this region too. The threshold for double ionization of Ar by electron and positron impact is correctly described, as compared to the data.

At high energies ($E > 1$ keV) our curves are below most of the electron-impact and proton-impact data. It is worth to mention that all the Ar shells have been included in this calculation, even the K-shell. So this unexplained undervalue of the theory may be related to the empirical branching ratios employed.

Ar triple ionization

In figure 6 the triple ionization of Ar is displayed. The experimental data for heavy projectiles is rather well described, though overestimated around the maximum. The theory predicts antiproton values above the proton ones at the maximum of the cross section. Experimentally, the data for protons match well with the data for antiprotons.

In this figure we remark the importance of the PCI by including the direct triple ionization values (dashed double-dotted line) and the triple ionization including PCI (solid line) for electron impact ionization. As can be noted, PCI is correctly included. It is interesting to note a double-shoulder shape in the triple ionization by light projectiles. This is due to the passage from the energy region of direct ionization (only valence-shell ionization) to the region of higher energies, where PCI is not negligible (inner shell ionization). Note that this double shoulder can be observed also in the electron impact measurements. The theory reproduces the shape but overestimates below 250 eV. It would be interesting to have measurements of triple ionization by positron impact to study this effect too.

Ar quadruple ionization

In figure 7 the quadruple ionization cross sections of Ar are displayed. Again we emphasize the importance of PCI by including the direct quadruple ionization for the electron-impact case (dashed double-dotted curve). Above 300 eV the PCI is crucial, instead the direct ionization falls down, being negligible for impact energies above 400 eV. The theory predicts a small shoulder around 200 eV related to these two different ionization mechanisms. It can also be noted that the threshold for electron-impact quadruple ionization is nicely described.

Figure 7 shows that there are no antiparticle data for quadruple ionization of Ar. This is related to the difficulties to measure such low values, i. e. around or less than 10^{-18} cm² for proton impact, around or less than 10^{-19} cm² for electron impact.

Ar quintuple ionization

Finally in figure 8 the quintuple ionization of Ar is displayed. The only data available in the literature is for electron-impact quintuple ionization. Nevertheless we include the CDW-EIS results for the four $|Z| = 1$ projectiles. Hopefully, these cross sections could be tested with future measurements by proton, antiproton and positron impact.

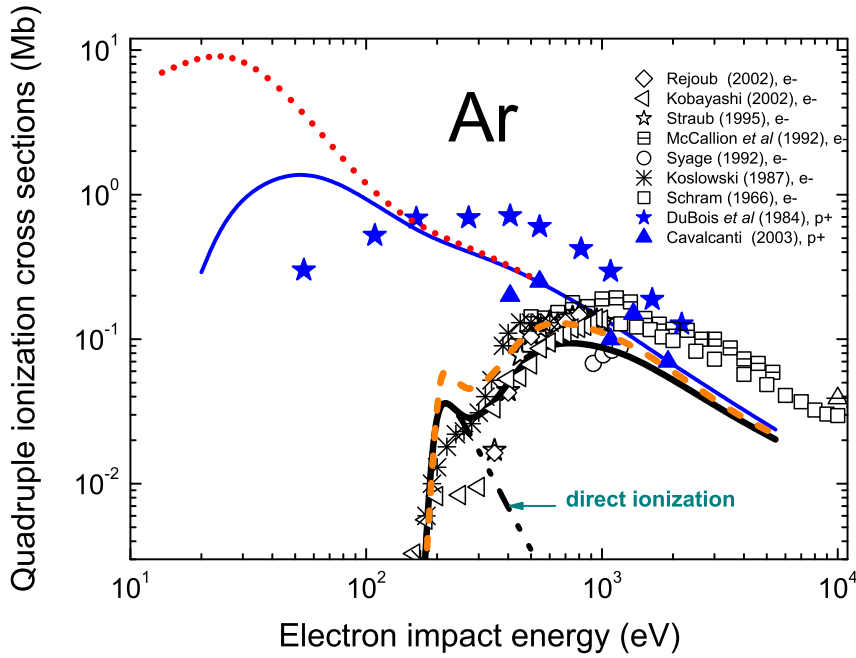


Figure 7: Quadruple ionization of Ar by $|Z| = 1$ projectiles as a function of the impact energy, considering equal velocity for heavy and light particles. Curves: CDW-EIS results for proton (blue thin solid line), antiproton (red dotted line), electron (black thick solid line) and positron (orange dashed-line) impact. Symbols: details in the inset; the references are: for protons p+ [9, 15], and for electrons e- [21, 23, 25, 26, 27, 28, 31, 32].

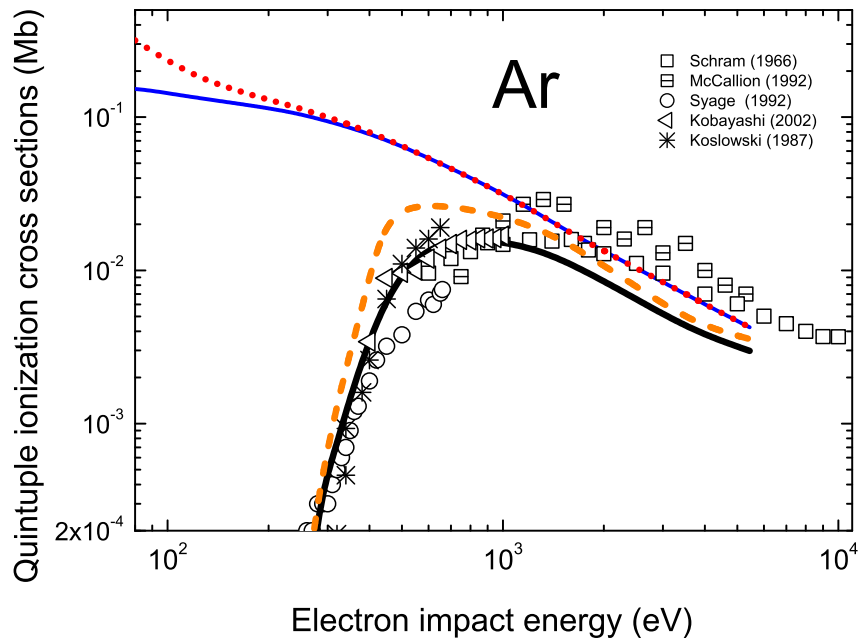


Figure 8: Quintuple ionization of Ar by $|Z| = 1$ projectiles as a function of the impact energy, considering equal velocity for heavy and light particles. Curves: CDW-EIS results for proton (blue thin solid line), antiproton (red dotted line), electron (black thick solid line) and positron (orange dashed-line) impact. Symbols: details in the inset; the references for electrons e^- are [21, 23, 26, 27, 31, 32].

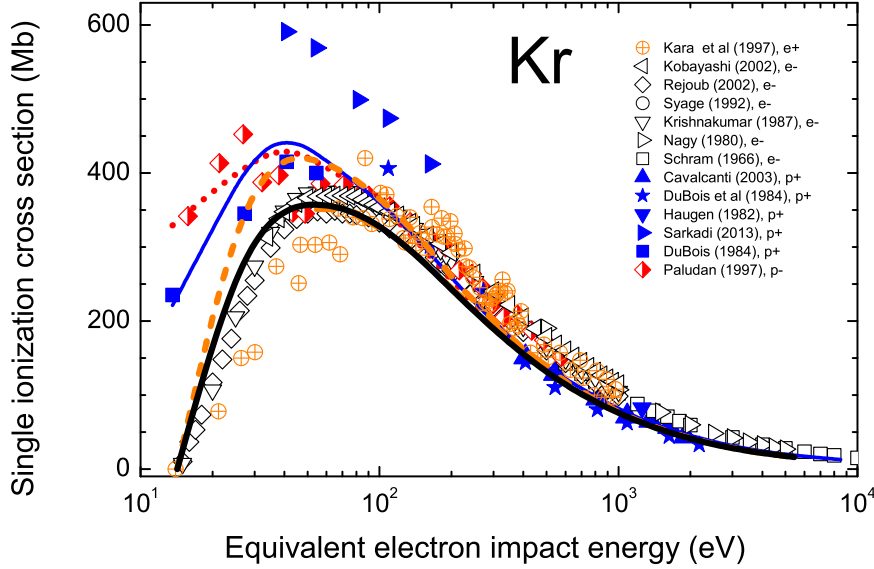


Figure 9: Single ionization of Kr by $|Z| = 1$ projectiles as a function of the impact energy, considering equal velocity for heavy and light particles. Curves: CDW-EIS results for proton (blue thin solid line), antiproton (red dotted line), electron (black thick solid line) and positron (orange dashed-line) impact. Symbols: details in the inset; the references are: for protons p+ [6, 9, 14, 15, 20], for electrons e- [21, 22, 23, 24, 25, 26], for positrons e+ [45], and for antiprotons p- [35].

The theoretical description is very good considering it is quintuple ionization of Ar in an IPM approximation. The prediction of the threshold at 230 eV is also fine. In this figure, the cross sections by electron and positron impact are entirely due the PCI following inner-shell ionization (1s, 2s, and 2p). And this is valid in the whole energy range, even just above the threshold. The direct-ionization contribution is so small that it is out of scale in figure 8, i.e. less than $2 \cdot 10^{-22} \text{ cm}^2$.

0.3.3 The multiple ionization of Kr

We present in this section a comparative study of Kr multiple ionization by the four $|Z| = 1$ projectiles, covering from single up to quintuple ionization. In figures 9-13 we displayed together the CDW-EIS results for proton, antiproton, electron and positron [52, 13, 53], and the available experimental data.

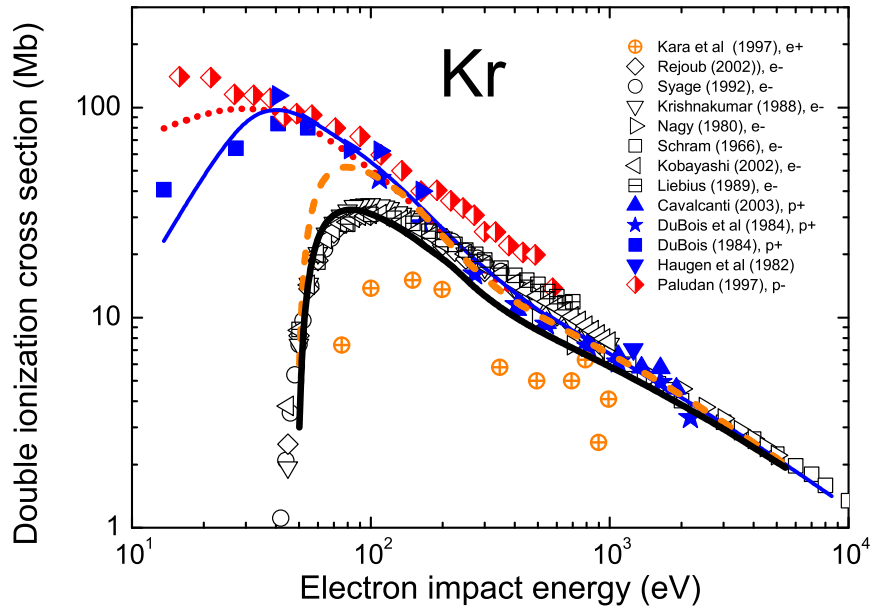


Figure 10: Double ionization of Kr by $|Z| = 1$ projectiles as a function of the impact energy, considering equal velocity for heavy and light particles. Curves: CDW-EIS results for proton (blue thin solid line), antiproton (red dotted line), electron (black thick solid line) and positron (orange dashed-line) impact. Symbols: details in the inset; the references are: for protons p+ [6, 8, 9, 14, 15, 17, 18, 16, 19], for electrons e- [21, 22, 23, 24, 25, 26, 30], for positrons e+ [45], and for antiprotons p- [35].

Kr single ionization

In figure 9 we display the single ionization cross sections of Kr. The theoretical-experimental agreement is very good. Note that for electron impact the theoretical description agrees in the maximum and in the energy threshold. Above 100 eV all the data seem to converge. Similarly to the case of Ar, the data by Sarkadi *et al* [20] for proton impact are quite above the CDW-EIS predictions. But in this case we can also compare with the measurements by DuBois and coworkers [6, 17]. DuBois experiments separate capture and pure ionization. The differences between Sarkadi *et al* [20] and DuBois data [6, 17] below 60 eV are clear. This seems to confirm the presence of capture in [20].

Kr double ionization

In figure 10 we can observe and analyze the double ionization of Kr by particle and antiparticle impact. The good description of Kr double ionization by antiproton, proton and electron impact is remarkable. The theoretical and experimental values show clearly that the cross sections for heavy projectiles are quite similar for impact velocities above 1.7 a.u.

The theoretical results show that the double ionization cross sections by the light projectiles are much lower than those of the heavy projectiles at intermediate energies, with the threshold around 40 eV. These values reproduce the electron impact data rather well. However, the positron data by Kara *et al* [45] are below the theoretical predictions and quite below the electron data.

At low impact energies the mass-effect dominates. The cross sections by light projectiles are below the heavy projectiles ones, with the characteristic sharp threshold. This contrasts with the charge-effect at high energies. Above 100 eV positron values are closer to proton values than to electron ones. The high energy convergence of the different curves and data is evident at high energies, as expected.

Kr triple ionization

The theoretical results presented in figure 11 nicely describe the measurements of proton, antiproton and electron impact. No measurements for triple ionization of Kr by positrons have been reported yet. For light projectiles, PCI is the main contribution almost in the whole energy range. This is remarked in figure 11 with a separate curve that shows the direct triple ionization without PCI. Again, the small hump near the threshold is associated with the appearance of the PCI contribution. It is present in the theoretical curve for electron impact, and may be noted in the certain data. The bigger hump for positron impact

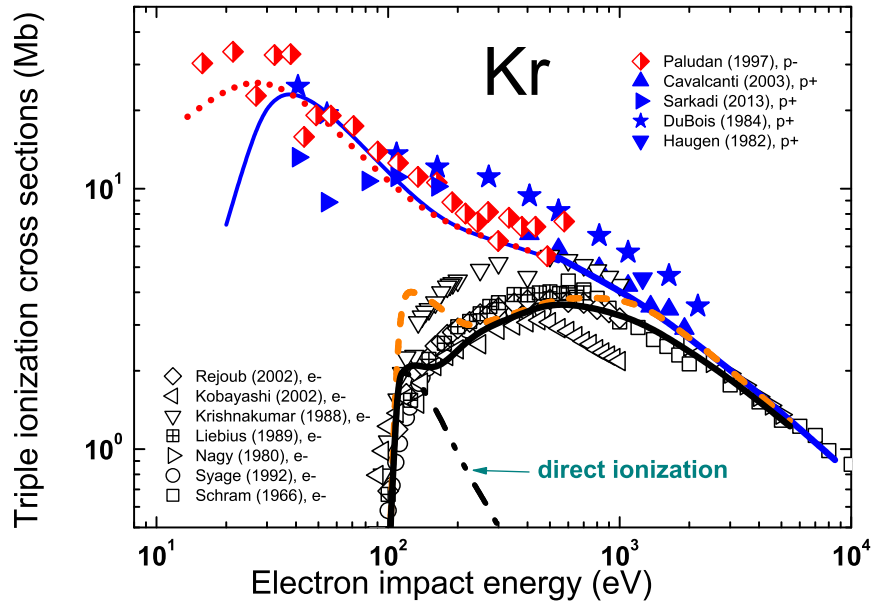


Figure 11: Triple ionization of Kr by $|Z| = 1$ projectiles as a function of the impact energy, considering equal velocity for heavy and light particles. Curves: CDW-EIS results for proton (blue thin solid line), antiproton (red dotted line), electron (black thick solid line) and positron (orange dashed-line) impact. Symbols: details in the inset; the references are: for protons p+ [9, 14, 15, 20], for electrons e- [21, 22, 23, 24, 25, 26, 30], and for antiprotons p- [35].

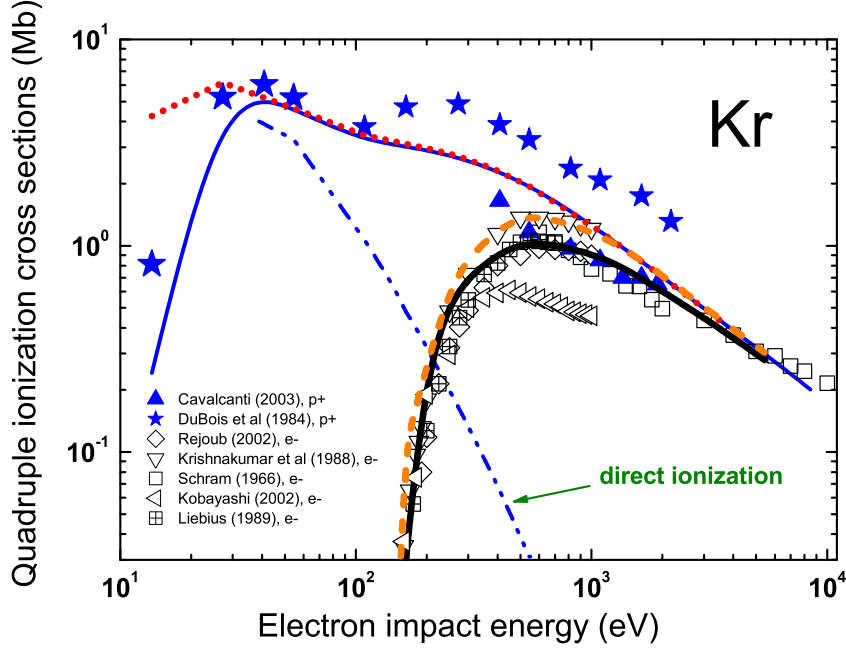


Figure 12: Quadruple ionization of Kr by $|Z| = 1$ projectiles as a function of the impact energy, considering equal velocity for heavy and light particles. Curves: CDW-EIS results for proton (blue thin solid line), antiproton (red dotted line), electron (black thick solid line) and positron (orange dashed-line) impact. Symbols: details in the inset; the references are: for protons p+ [9, 15], and for electrons e- [21, 24, 25, 26, 30].

could be an artifact of the theoretical calculations. However, no theoretical experimental comparison is possible for positron impact.

As already mentioned, the mass effect is more important than the charge effect at low and intermediate energies, while equal charge determines the energy for which the curves converge. Theoretically, the positron cross sections tend to proton ones for $E > 1$ keV. Instead electron impact cross sections converge to the rest above 2 keV. This may indicate that when the ionization of inner shells dominates, the mass effect prevails over the charge effect.

Kr quadruple ionization

Figure 12 shows the quadruple ionization of Kr. The theoretical-experimental agreement is noticeable. The comparison is very interesting. The direct ioniza-

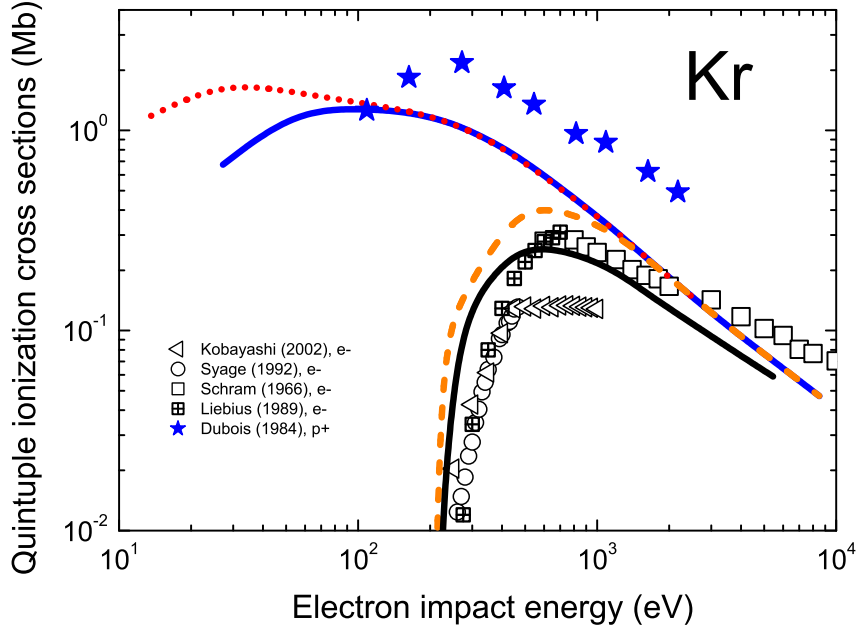


Figure 13: Quintuple ionization of Kr by $|Z| = 1$ projectiles as a function of the impact energy, considering equal velocity for heavy and light particles. Curves: CDW-EIS results for proton (blue thin solid line), antiproton (red dotted line), electron (black thick solid line) and positron (orange dashed-line) impact. Symbols: details in the inset; the references are: for protons p+ [15], and for electrons e- [21, 23, 26, 30].

tion is a minor contribution for light particles even near the energy threshold. In the case of heavy particles, PCI is important at rather low energies. This is remarked in figure 12 by including the theoretical direct quadruple ionization cross section by proton impact. Below 700 eV the theoretical results for positron impact are close to the electron ones, but no comparison with the experiments is possible for positron impact. The lack of antiparticle cross sections is evident in this figure. We expect that the present study may be of interest for future measurements.

Kr quintuple ionization

Finally, the quintuple ionization is displayed in figure 13. The behavior is similar to the one observed for quadruple ionization. Note that for proton

impact there is only one set of experimental data, by DuBois [6]. The case is different for electron impact measurements, which are by far the most abundant of the four projectiles studied here. However, we included the theoretical predictions for the four $|Z| = 1$ projectiles in view of future measurements.

For electron impact, PCI dominates the quintuple ionization in the whole energy range. The direct quintuple ionization is negligible even for energies near the threshold. It is worth to mention that to describe the quintuple ionization of Kr, even the ionization of the L-shell must be considered [68]. Moreover, the good performance of the CDW-EIS for the Kr^{+5} final charge state is due to the correct description of the ionization probabilities of the very deep shells, both by heavy and light projectiles.

0.3.4 The multiple ionization of Xe

Finally, Xenon multiple ionization by $|Z| = 1$ projectiles is displayed in figures 14-18, from single to quintuple ionization. The results for multiple ionization of Xe in these figures show the scope of the model that combines CDW-EIS, IPM for multiple ionization, mass effects in the description of light projectiles and the PCI through the empirical branching ratios. The theoretical results for Xe show a very good description of the experimental measurements for the different $|Z| = 1$ projectiles, meaning that the charge effects (positive vs. negative charges, repulsive or attractive potential) and the mass effects (difference in the impact energy, threshold, non-linear trajectories) are correctly included. On the other hand, it is reasonable that the IPM approximation (no electron-electron correlation, no changes in the target potential due to the loss of one or more electrons) works better for Xe with 54 electrons than for Ne, with only 10 electrons. The Xe potential is less affected by the loss of a few electrons, and the approximation of independent events without changes is more realistic.

Xe single ionization

In Figure 14 the ionization of just one electron is displayed in linear scale in order to show in detail the measurements and the theoretical cross sections around the maximum. The CDW-EIS predicts that proton and antiproton maximum cross sections are around 40 eV (in electron impact energy, it is $v \sim 1.7$ a.u.), while positron and electron curves are shifted to 55-60 eV. It is very interesting that the positron and antiproton highest cross sections are almost equal. The electron impact values are below the positron data around the maximum. For impact energies 40-80 eV, the single ionization by positron-impact is more effective (higher probabilities) than by electron-impact.

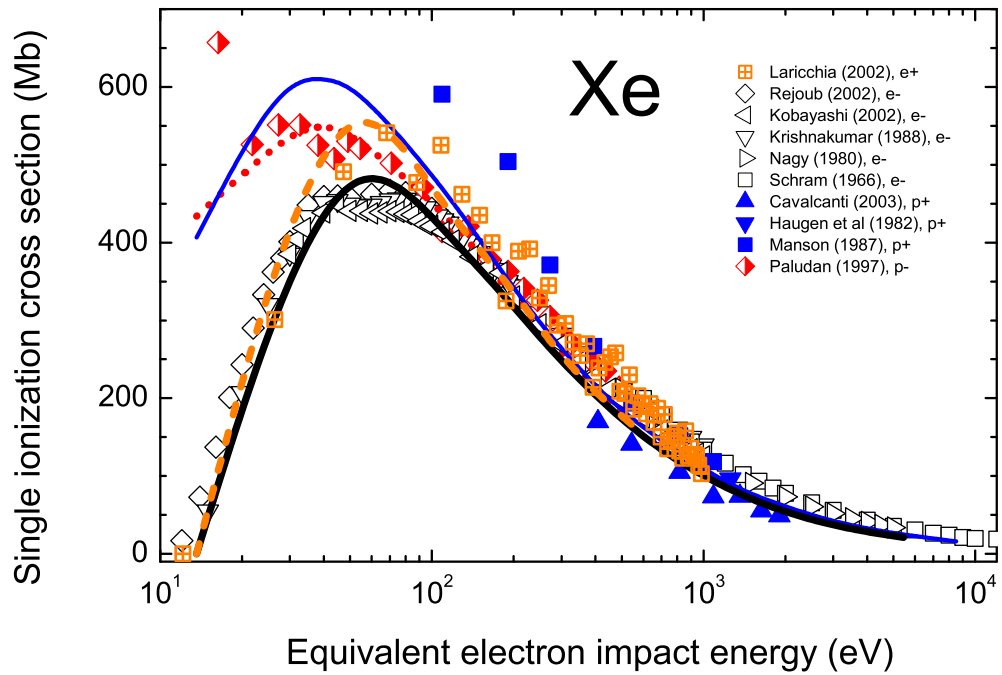


Figure 14: Single ionization of Xe by $|Z| = 1$ projectiles as a function of the impact energy, considering equal velocity for heavy and light particles. Curves: CDW-EIS results for proton (blue thin solid line), antiproton (red dotted line), electron (black thick solid line) and positron (orange dashed-line) impact. Symbols: details in the inset; the references are: for protons p+ [9, 14, 18], for electrons e- [21, 22, 23, 24, 25, 26], for positrons e+ [42], and for antiprotons p- [35].

The very good agreement with the experimental values reinforce these conclusions. The measurements for the different projectiles converge at high energies, and show the peculiar behavior for each projectile at lower energies. The description of the antiproton measurements by Paludan *et al* [35] is quite good in the whole energy range. The same for electron and positron impact. Clearly the positron measurements are above the electron ones, as predicted theoretically, with values very similar to those of antiproton. The experimental data for proton impact by Manson *et al* [18] are well described at high energies, but the three measurements for impact velocities $v < 3$ a.u. are clearly above the theoretical curve. The comparison of them with the single ionization by antiproton, which is actually pure ionization, suggests that electron capture may be present in this proton impact data. At high energies, the measurements of single ionization of Xe by proton impact by Cavalcanti *et al* [9] are below the rest. It would be useful to compare measurements for Xe^+ production by proton impact at $1 \leq v \leq 4$ with the similar antiproton values.

Xe double ionization

The agreement between the theoretical and the experimental values in figure 15 is amazing. These cross sections are not so small, i.e. around $10^{-15} - 10^{-16}$ cm^2 . The experimental values for double ionization of Xe by antiprotons are very interesting because they cover the energy range around the maximum of the cross section. Instead, there is a lack of proton impact data in this energy region (velocity $v < 3$ a.u.). For positron impact, there are three groups of independent data with rather good agreement with the CDW-EIS results. It may be noted that the low energy measurements by Bluhme *et al*[48] suggest a different energy threshold for electron and positron impact. This is not shown by the theory [56, 53] included here. However, it is worth to remember here that the CDW-EIS is not expected to be valid near the energy threshold. So we cannot state a conclusion about this positron-electron difference.

Above 1 keV all the double ionization cross sections converge. These values are highly influenced by the single ionization of a subvalence electron followed by decay and emission of a second electron. This PCI is important for energies above 200 eV and represents 80% of the double ionization cross section at 1 keV.

Xe triple ionization

The triple ionization of Xe, theory and compilation of available data, is presented in figure 16. The comparison shows again the validity of the description. The antiproton, proton and electron impact data are in reasonable agreement

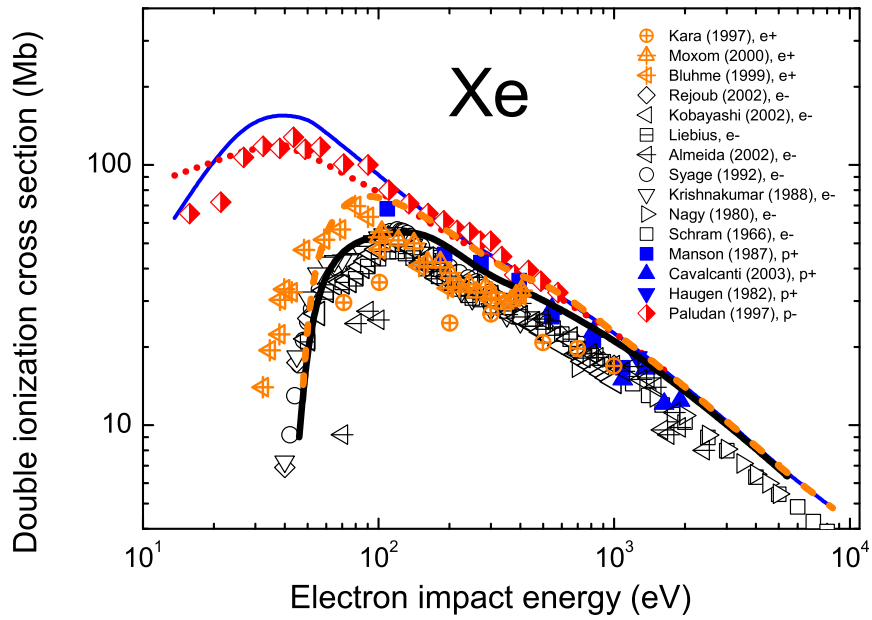


Figure 15: Double ionization of Xe by $|Z| = 1$ projectiles as a function of the impact energy, considering equal velocity for heavy and light particles. Curves: CDW-EIS results for proton (blue thin solid line), antiproton (red dotted line), electron (black thick solid line) and positron (orange dashed-line) impact. Symbols: details in the inset; the references are: for protons p+ [9, 14, 18], for electrons e- [21, 22, 23, 24, 25, 26, 29, 30], for positrons e+ [45, 49, 48], and for antiprotons p- [35].

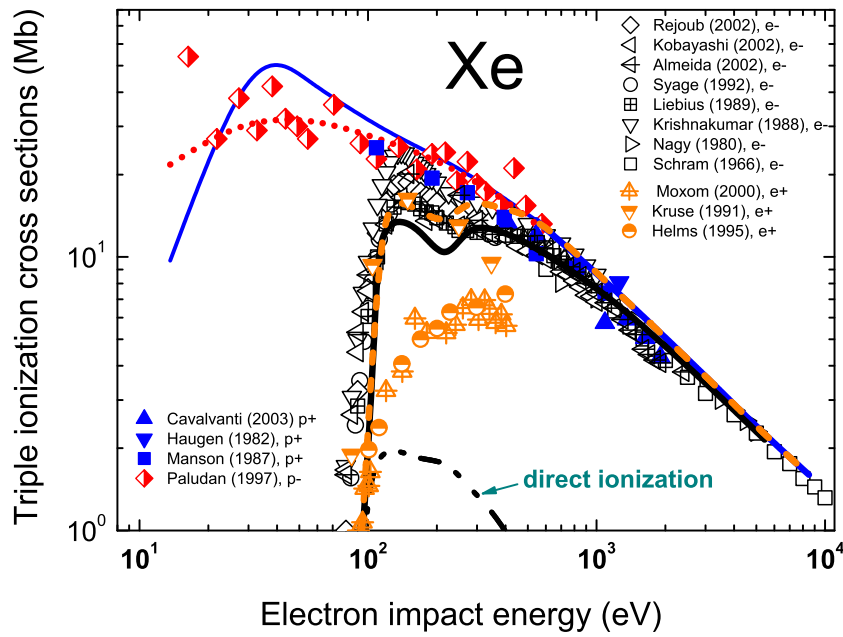


Figure 16: Triple ionization of Xe by $|Z| = 1$ projectiles as a function of the impact energy, considering equal velocity for heavy and light particles. Curves: CDW-EIS results for proton (blue thin solid line), antiproton (red dotted line), electron (black thick solid line) and positron (orange dashed-line) impact. Symbols: details in the inset; the references are: for protons p+ [9, 14, 18], for electrons e- [21, 22, 23, 24, 25, 26, 29, 30], for positrons e+ [49, 50, 51], and for antiprotons p- [35].

with the theoretical curves. For triple ionization, the threshold for light projectile ionization is very sharp and pushes down the cross sections. Theoretically, the cross sections are similar for electron and positron impact, with the two humps and a small minimum at 200 eV. At high energies, the positron curve converges to proton one at 400 eV, while the electron curve does above 1 keV. This high energy triple ionization is mostly PCI, as indicated in the figure. The curve obtained just considering the direct triple ionization (without PCI) is far from describing the data.

It can be noted in figure 16 that there are differences among the three sets of positron data. The measurements by Kruse *et al* [51] agree with the expected values around the maximum. However, the more recent measurements by Moxom *et al* [49] and Helms *et al* [50] are below the curves and the electron-impact data. Again we can draw attention to the lack of proton impact measurements at intermediate and low energies.

Xe quadruple ionization

In the figure 17 the quadruple ionization of Xe is displayed, including the experimental data available and the CDW-EIS results for the four $|Z| = 1$ projectiles. The abundance of electron impact data can be noted, while there is only one set for positron impact [49], and only one set for proton impact [9]. No antiproton values are available in the literature, and proton data is available only in the energy region where they converge to electron-impact ones. The lack of measurements for the heavy projectiles around the maximum of the cross section does not allow to evaluate the theoretical predictions for proton and antiprotons. On the other hand, the positron measurements by Moxom *et al* [49] are a factor 2 below the theoretical values.

The agreement with the electron impact data below 300 eV is fine considering they are quadruple-ionization cross sections. On the contrary, the theoretical high-energy values are too small. Concerning this undervalue, the CDW-EIS results in [53] include very deep shells, so the branching ratios of PCI may be the reason. However, it is fair to remark that at 5 keV the direct quadruple ionization cross sections are 4 orders of magnitude below the experimental values. Thus, the theoretical values including PCI, even a factor two below the data at 5 keV, are a rather good description of the electron impact values.

Xe quintuple ionization

Finally, for quintuple ionization of Xe in figure 18, only electron and proton impact data are available in the literature. For electron impact, the theoretical curve is in good agreement with the experimental measurements, considering

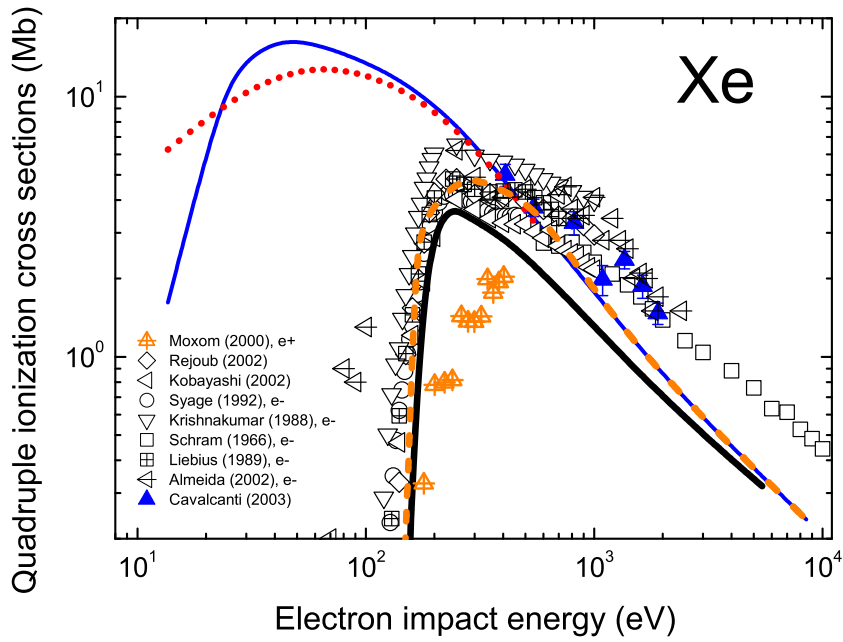


Figure 17: Quadruple ionization of Xe by $|Z| = 1$ projectiles as a function of the impact energy, considering equal velocity for heavy and light particles. Curves: CDW-EIS results for proton (blue thin solid line), antiproton (red dotted line), electron (black thick solid line) and positron (orange dashed-line) impact. Symbols: details in the inset; the references are: for protons p+ [9], for electrons e- [21, 23, 24, 25, 26, 29, 30], and for positrons e- [49].

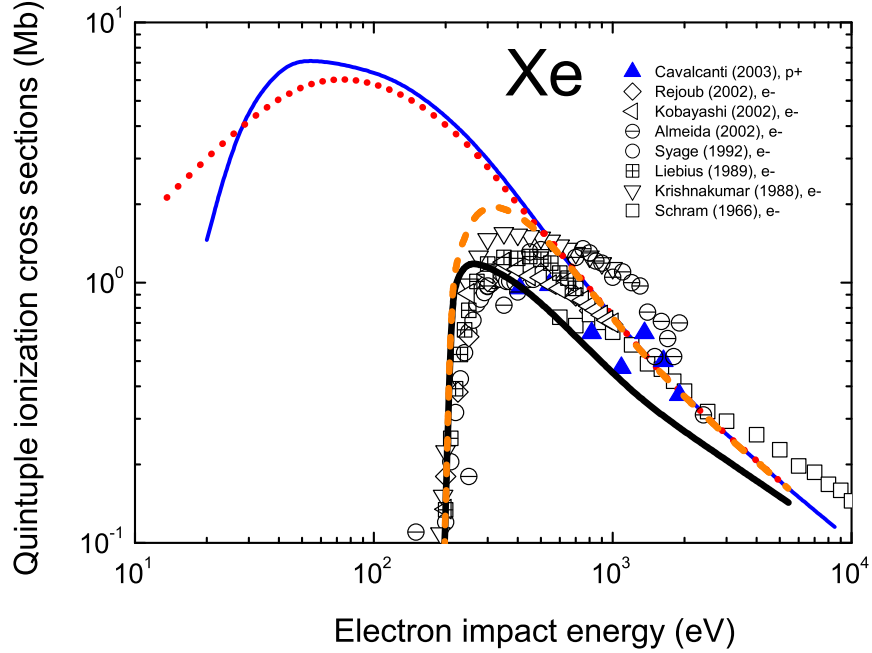


Figure 18: Quintuple ionization of Xe by $|Z| = 1$ projectiles as a function of the impact energy, considering equal velocity for heavy and light particles. Curves: CDW-EIS results for proton (blue thin solid line), antiproton (red dotted line), electron (black thick solid line) and positron (orange dashed-line) impact. Symbols: details in the inset; the references are: for protons p+ [9], and for electrons e- [21, 23, 24, 25, 26, 29, 30].

the difficulties of such low values. The high energy proton measurements by Cavalcanti *et al* [9] also agree with the electron data, except with those by Almeida *et al* [29] that are larger than the rest. The theoretical curves for proton and antiproton impact are quite similar around the maximum. But there is no experimental data to confirm this.

There are some characteristics to remark about the CDW-EIS results for quintuple ionization displayed in figure 18: the first one is that at low impact energies, the energy threshold for electron and positron impact is nicely described. The inclusion of the mean energy transferred in the threshold for multiple ionization proved to be important [56]. For example, while the outer 5s and 5p electrons of Xe have binding energies around 13 eV, the threshold for quintuple ionization is 178 eV [53], much greater than 5×13 eV. The second point to emphasize is that the Auger-like processes leading to quintuple ioniza-

tion are by far the main contribution for light projectiles in the whole energy range, even near the threshold. The single ionization of the Xe 4s, 3d, and 3p electrons are the most important contributions to final quintuple ionization. This is clear in view of the experimental branching ratios for Xe in table 4 of [13]. At high energies, again the convergence of positron values to proton and antiproton takes place around 400 eV, while electron impact values do so only above 6 keV.

0.4 Concluding remarks and future prospects

In this chapter the particle and antiparticle multiple ionization of Ne, Ar, Kr and Xe was analyzed considering heavy and light projectiles. This was done based on the CDW-EIS results and a vast compilation of the experimental data available in the literature for the sixteen collisional systems, four projectiles and four targets.

The theoretical formalism combines the independent particle model, the CDW-EIS ionization probabilities for heavy projectiles, the changes in this approximation to consider light-particle collisions (difference in the impact energy, threshold, non-linear trajectories), and the inclusion of the post-collisional contribution to the final charge state due to Auger-like processes.

The multiple ionization of Kr and Xe shows the scope of the model: good description for the different $|Z| = 1$ projectiles, meaning that the charge and mass effects are correctly included. The improvement of the theoretical results with the target nuclear charge (or with the number of bound electrons) is evident. The employment of the independent particle model to obtain multiple ionization probabilities does not consider changes in the target potential due to the loss of one or more electrons. It is reasonable that this approximation works better for atoms such as Kr or Xe than for Ne.

The correction of the CDW-EIS approximation to describe light particles shows the tendency of the experimental data. On the other hand, the energy thresholds calculated separately and imposed within the multinomial expansion, proved to describe rather well the experimental values for electron and positron impact. Although the threshold itself is rather well described, the CDW-EIS approximation is not expected to be valid for low energies.

The highly-charged ion production is dominated by the post-collisional electron emission that follows the inner-shell ionization (rearrangement and/or Auger processes). The CDW-EIS results are good even for quadruple and quintuple ionization cross sections. These calculations are sensitive to the good description of the deep shell ionization. They also rely on the empirical branching ratios of post-collisional ionization. We concluded that in multiple ionization by light particles, the post-collisional contribution is the main ionization channel in the whole energy range, even close to the threshold.

Future prospects can be separated in two lines. Within the theoretical work, the case of Ne is one of the limitations of the model. Not only related to the independent electron approximation, but also to the inclusion of the shake-off. Future progress in this regard is expected. On the other hand, the CDW-EIS has already been tested for sextuple ionization of Kr and Xe by electron impact with very good agreement with the experimental data. The extension to higher ionization orders (final charge state $+q \geq 7$) requires high

computational effort but is possible.

Within the experimental research, the extensive compilation of data and the comparison of electron, positron, proton and antiproton values have been very enlightening. Unfortunately, the thorough particle-antiparticle comparison could be made up to double ionization. This is an interesting point to consider for future research. There are no positron impact experiments for higher levels of multiple ionization of rare gases. The exception is Xe. The antiproton data available goes up to triple ionization. It is interesting to note that, though the requirements and difficulties of the antiproton experiments (high energy physics facility), there are more measurements for ionization of Xe by antiprotons than by protons.

Present review also discussed the normalization of antiparticle relative measurements to the high energy electron ionization cross sections. We found that at high energies, the ionization cross sections by antiparticles impact converge to proton impact values at lower energies rather than to electron impact ones. Recent techniques for electron ionization measurements introduce very low relative errors, and make them quite interesting and reliable for the normalization purposes. The point to consider is that from which impact energy positron and electron, or antiproton and electron ionization cross sections, are equal.

Acknowledgments

This work was partially supported by the following institutions in Argentina: Consejo Nacional de Investigaciones Científicas y Técnicas, Agencia Nacional de Promoción Científica y Tecnológica, and Universidad de Buenos Aires. I thank Jorge Miraglia for useful discussions on the theoretical results.

Bibliography

- [1] McGuire J H 1986 *Positron (Electron)-Gas Scattering*, eds. Kauppila W E, Stein T S and Wadehra J M (Singapore, World Scientific) 222-231
- [2] Schultz D R, Olson R E and Reinhold C O 1991 *J. Phys. B: At. Mol. Opt. Phys.* **24** 521-558
- [3] Knudsen H and Reading J F 1992, *Phys. Report* **212** 107-222
- [4] Knudsen H and Reading J F 1992 *Phys. Rep.* **212** 107-222
- [5] Paludan K, Laricchia G, Ashley P, Kara V, Moxom J, Bluhme H, Knudsen H, Mikkelsen U, Möller S P, Uggerhøj U, and Morenzoni E 1997, *J. Phys. B: At. Mol. Opt. Phys.* **30** L581-L587
- [6] DuBois R D 1984, *Phys. Rev. Lett* **52**, 2348-2351
- [7] G Laricchia, Cooke D A, Köver A, Brawley S J 2013 *Experimental Aspects of Ionization Studies by Positron and Positronium Impact* (Cambridge University Press) **56** 116-136
- [8] Cavalcanti E G, Sigaud G M, Montenegro E C, Sant 'Anna M M, and Schmidt-Bocking H 2002 *J. Phys. B: At. Mol. Opt. Phys.* **35** 3937-3944
- [9] Cavalcanti E G, Sigaud G M, Montenegro E C, and Schmidt-Bocking H 2003 *J. Phys. B: At. Mol. Opt. Phys.* **36** 3087-3096
- [10] Spranger T and Kirchner T 2004 *J. Phys. B: At. Mol. Opt. Phys.* **37** 4159
- [11] Galassi M E, Rivarola R D, and Fainstein P D 2007, *Phys. Rev. A* **75**, 052708
- [12] Montanari C C, Montenegro E C and Miraglia J E 2010, *J. Phys. B: At. Mol. Opt. Phys.* **43**, 165201
- [13] Montanari C C and Miraglia J E 2014, *J. Phys. B: At. Mol. Opt. Phys.* **47**, 105203.
- [14] Haugen H K, Andersen L H, Hvelplund P and Knudsen H 1982, *Phys. Rev A* **26** 1962-1974
- [15] DuBois R D, Toburen L H and Rudd M E 1984 *Phys. Rev. A* **29** 70-76
- [16] Andersen L H, Hvelplund P, Knudsen H, Möller S P, Sørensen A H, Elsener K, Rensfelt K G and Uggerhøj 1987 *Phys. Rev. A* **36** 3612-3629
- [17] DuBois R D and Manson S T 1987 *Phys. Rev. A* **35** 2007-2025
- [18] Manson S T and DuBois R D 1987 *J. Physique* **48** C9 263-266 (online by EDP Sciences <http://dx.doi.org/10.1051/jphyscol:1987945>)
- [19] Gonzalez A D and Horsdal Pedersen E 1993, *Phys. Rev. A* **48** 3689
- [20] Sarkadi L, Herczku P, Kovacs S T S, and Kover A 2013, *Phys. Rev A* **87** 062705

- [21] Schram B L, Boerboom A J H and Kistemaker J 1966 *Physica* **32** 185-196; Schram B L 1966 *Physica* **32** 197-209; Schram B L, de Heer F J, Van der Wiel M J and Kistemaker J 1965 *Physica* **31** 94; Adamczyk B, Boerboom A J H, Schram B L and Kistemaker J 1966 *J. Chem. Phys.* **44** 4640-4642
- [22] Nagy P, Skutlartz A and Schmidt V 1980, *J. Phys. B: At. Mol. Opt. Phys.* **13** 1249-1267
- [23] Syage J A 1992, *Phys. Rev. A* **46** 5666
- [24] Krishnakumar E and Srivastava S K 1988, *J. Phys. B: At. Mol. Opt. Phys.* **21** 1055-1082
- [25] Rejoub R, Lindsay B G and Stebbing R F 2002, *Phys. Rev. A* **65** 042713
- [26] Kobayashi A, Fujiki G, Okaji A and Masuoka T 2002 *J. Phys. B: At. Mol. Opt. Phys.* **35** 2087-2103
- [27] McCallion P, Shah M B and Gilbody H B 1992, *J. Phys. B: At. Mol. Opt. Phys.* **25** 1061-1071
- [28] Straub H C, Renault P, Lindsay B G, Smith K A and Stebbings R F 1995, *Phys. Rev. A* **52** 1115-1124
- [29] Almeida D P, Fontes A C and Godinho C F L 1995, *J. Phys. B At. Mol. Opt. Phys.* **28** 3335-3345
- [30] Liebius H, Binder J, Koslowski H R, Wiesemann K and Huber B A 1989, *J. Phys. B: At. Mol. Opt. Phys.* **22** 83-97
- [31] Singh R K, Hippler R and Shanker R 2002, *J. Phys. B: At. Mol. Opt. Phys.* **35** 3243-3256.
- [32] Koslowski H R, Binder J, Huber B A and Wiesemann K 1987, *J. Phys. B: At. Mol. Opt. Phys.* **20**, 5903
- [33] Andersen L H, Hvelplund P, Knudsen H, Möller S P, Elsener K, Rensfelt K G and Uggerhøj 1986, *Phys. Rev. Lett* **57** 2147-2150
- [34] Andersen L H, Hvelplund P, Knudsen H, Möller S P, Pedersen J O P, Tang-Pedersen S, Uggerhøj E, Elsener K and Morenzoni E 1989, *Phys. Rev. A* **40** 7366
- [35] Paludan K, Bluhme H, Knudsen H, Mikkelsen U, Möller S P, Uggerhøj E and Morenzoni E 1997, *J. Phys. B: At. Mol. Opt. Phys.* **30** 3951
- [36] Knudsen H et al 2008, *Phys. Rev. Lett* **101** 043201 107-222
- [37] Knudsen H et al 2009, *Nucl. Instrum and Meth. in Phys. Research Section B* **267** 244-247
- [38] Kirchner T and Knudsen H 2011, *J. Phys. B: At. Mol. Opt. Phys.* **44** 122001
- [39] Knudsen H, Brun-Nielsen L, Charlton M and Poulsen M R 1990, *J. Phys. B: At. Mol. Opt. Phys.* **23** 3955-3976
- [40] Jacobsen F M, Frandsen N P, Knudsen H, Mikkelsen U and Schrader D M 1995, *J. Phys. B: At. Mol. Opt. Phys.* **28** 4691-4695
- [41] Mori S and Sueoka O 1994, *J. Phys. B: At. Mol. Opt. Phys.* **27**, 4349-4364
- [42] Laricchia G, Van Reeth P, Szuinska M and Moxom J 2002, *J. Phys. B: At. Mol. Opt. Phys.* **35** 2525-2540
- [43] Marler J P, Sullivan J P, Surko C M 2005, *Phys. Rev. A* **71** 022701
- [44] M Charltoni, L Brun-Nielsen, B I Deutch, P Hvelplund, F M Jacobsen, H Knudsen, G Laricchiati and M R Poulsen 1989, *J. Phys. B: At. Mol. Opt. Phys.* **22** 2779-2788
- [45] Kara V, Paludan K, Moxom J, Ashley P and Laricchia G 1997, *J. Phys. B: At. Mol. Opt. Phys.* **30** 3933-3949

- [46] Moxom J, Ashley P and Laricchia G 1996, *Can. J. Phys.* **74** 367
- [47] Moxom J, D. M. Schrader, G. Laricchia, Jun Xu, and L. D. Hulett 1999 *Phys. Rev. A* **60** 2940-2943
- [48] Bluhme H, Knudsen H, Merrison J P and Nielsen K A 1999, *J. Phys. B: At. Mol. Opt. Phys.* **32** 5237
- [49] Moxom J 2000, *J. Phys. B: At. Mol. Opt. Phys.* **33** L481-L485
- [50] Helms S, Brinkmann U, Deiwiks J, Hippler R, Schneider H, Segers D and Paridaens J 1995, *J. Phys. B: At. Mol. Opt. Phys.* **28** 1095
- [51] Kruse G, Quermann A, Raith W, Sinapius G and Weber M 1991 *J. Phys. B: At. Mol. Opt. Phys.* **24** L33
- [52] Montanari C C and Miraglia J E 2012, *J. Phys. B: At. Mol. Opt. Phys.* **45**, 105201
- [53] Montanari C C and Miraglia J E 2015, *J. Phys. B: At. Mol. Opt. Phys.* **48**, 165203.
- [54] Miraglia J E and Gravielle M S 2008 *Phys. Rev. A* **78** 052705
- [55] Fainstein P D, Ponce V H and Rivarola R D 1988, *J. Phys. B: At. Mol. Opt. Phys.* **21**, 287
- [56] Montanari C C and Miraglia J E 2015, *J. Phys.: Conf. Ser.* **583** 012018
- [57] Santos A C F, Melo W S, Sant'Anna M M, Sigaud G M and Montenegro E C 2001, *Phys Rev A* **63** 062717
- [58] Sant'Anna M M, Luna H, Santos A C F, McGrath C, Shah M B, Cavalcanti E G, Sigaud G M and Montenegro E C 2003, *Phys Rev A* **68** 042707
- [59] Wolff W, Luna H, Santos A C F, Montenegro E C, DuBois R D, Montanari C C and Miraglia J E 2011, *Phys. Rev. A* **84**, 042704
- [60] Montanari C C, Miraglia J E, Wolff W, Luna H, Santos A C F, and Montenegro E C 2012, *J. Phys.: Conf. Ser.* **388** 012036.
- [61] Kirchner T, Horbatsch M and Lüdde H J 2001, *Phys. Rev. A* **64**, 012711; 2002, *Phys. Rev. A* **66**, 052719
- [62] Kirchner T, Santos A C F, Luna H, SantAnna M M, Melo W S, Sigaud G M, and Montenegro E C 2005, *Phys. Rev. A* **72** 012707.
- [63] Schenk G and Kirchner T 2009, *J. Phys. B: At. Mol. Opt. Phys.* **42** 205202
- [64] Schenk G, Horbatsch M and Kirchner T 2013, *Phys. Rev. A* **88**, 012712
- [65] Schenk G and Kirchner T 2015, *Phys. Rev. A* **91**, 052712
- [66] Tachino C A, Galassi M E and Rivarola R D 2008, *Phys. Rev. A* **77** 032714
- [67] Tachino C A, Galassi M E and Rivarola R D 2009, *Phys. Rev. A* **80** 014701.
- [68] Tavares A C , Montanari C C, Miraglia J E , and Sigaud G M 2014, *J. Phys. B: At. Mol. Opt. Phys.* **47**, 045201.
- [69] Archubi C D, Montanari C C, and Miraglia J E 2007, *J. Phys. B: At. Mol. Opt. Phys.* **40** 943
- [70] Rapp D and Englander-Golden P 1965, *J. Chem. Phys.* **43** 1464
- [71] Sorokin A A, Shmaenok L A, Bobashev S V, Möbus B, and Ulm G 1998, *Phys. Rev A* **58** 2900
- [72] Rudd M E, Kim Y-K, Madison D H and Gallagher J W 1985, *Rev. Modern Phys.* **57** 96594